

# Improved QE in CMOS image sensors with nano-black antireflection layer

Martin J. Prest  
School of Physical Sciences  
The Open University  
Milton Keynes, UK  
martin.prest@open.ac.uk

Ville Vähänissi  
Department of Electronics and  
Nanoengineering  
Aalto University  
Espoo, Finland  
ville.vahanissi@aalto.fi

Olli Setälä  
Department of Electronics and  
Nanoengineering  
Aalto University  
Espoo, Finland  
olli.setala@aalto.fi

Hele Savin  
Department of Electronics and  
Nanoengineering  
Aalto University  
Espoo, Finland  
hele.savin@aalto.fi

Konstantin D. Stefanov  
School of Physical Sciences  
The Open University  
Milton Keynes, UK  
konstantin.stefanov@open.ac.uk

Douglas Jordan  
Teledyne-e2v  
Chelmsford, UK  
douglas.jordan@teledyne.com

**Abstract**— A novel anti-reflection process is demonstrated which improves the quantum efficiency (QE) of a CMOS image sensor, with particular benefits at the ultraviolet (UV) and near infrared (NIR) ends of the electromagnetic spectrum. Also, the dark current and photoresponse non-uniformity (PRNU) were reduced to about 33% and 55%, respectively, of the values for a conventional control sensor. The nano-black anti-reflection layer was made using a reactive-ion-etch technique to form nano-scale spikes at the surface which greatly reduce the reflectivity of the surface, which has a matt-black appearance. The sensor used, a CIS115 from Teledyne-e2v, is a back-side-illuminated (BSI) device with  $\approx 10 \mu\text{m}$  active silicon thickness and  $2000 \times 1504$  pinned photodiode pixels with a pitch of  $7 \mu\text{m}$ . The improved QE is most impressive at UV wavelengths, below  $400 \text{ nm}$ , where the QE increases towards 100%, although no correction was made for an increased electron generation rate, as this is not easily quantified. This high QE result is compared with a conventional antireflection (AR) coating which shows a steep drop in QE below  $400 \text{ nm}$ . There is also an improvement in QE in the NIR (from  $700 \text{ nm}$  to  $1100 \text{ nm}$ ) for the nano-black sensor, and this is despite the approx.  $1 \mu\text{m}$  thinning of the silicon by the etching process, which would normally reduce the QE. Some of the QE improvement may be the result of increased scattering of the incident light, which is supported by the reduced PRNU.

**Keywords** — image sensor, CMOS, quantum efficiency, antireflection coating

## I. INTRODUCTION

Silicon image sensors are prone to poor QE at UV wavelengths because conventional surface passivation tends to be thicker than the absorption depth (only a few nm). Whereas at NIR wavelengths, the absorption depth required is 10s to 100s of  $\mu\text{m}$ , so thick layers are required. The CIS115 sensor [1] used in this work was optimised for high QE in the visible range and for high spatial resolution, so its active silicon thickness of  $10 \mu\text{m}$  is not very suitable for NIR use. However, an anti-reflection process which improves QE at both ends of the visible spectrum would enable more applications for conventional CMOS sensors, which are the world's widest used image sensor technology.

The nano-black process has previously demonstrated high QE in discreet photodiodes [2]. To the authors' knowledge, this is the first time that such a process has been applied to a monolithic CMOS image sensor. The nano-black antireflection layer was fabricated without modifying the standard BSI process, as a last step, in place of applying an AR coating. The nano-black fabrication process is a low-temperature ( $-120 \text{ }^\circ\text{C}$ ) reactive-ion plasma etch which produces a nano-structured surface of closely spaced spikes with average height  $500 \text{ nm}$  and width  $100 \text{ nm}$ . This surface then receives a conformal coating of  $20 \text{ nm Al}_2\text{O}_3$ , deposited by atomic layer deposition, with negative surface charge to provide a suitable electric field in the sensor. Fig. 1a shows an electron micrograph of the nano-structured silicon surface, the spike shapes cause multiple reflections between the structures, and this allows a gradual change in refractive index as light approaches the surface, improving the light absorption. Fig. 1b shows a CIS115 sensor with nano-black layer covering the lower half of the pixel array.

For QE measurements, nano-black sensors were compared to control sensors with a conventional multilayer AR coating for visible light. UV AR coatings were available [1], [3], but their QE was limited to 60% at UV and visible wavelengths, so the visible optimised AR coating (named by the manufacturer as multilayer-2) was chosen as a more suitable comparison.

For the dark current and PRNU measurements, comparison was made using a sensor where the nano-black

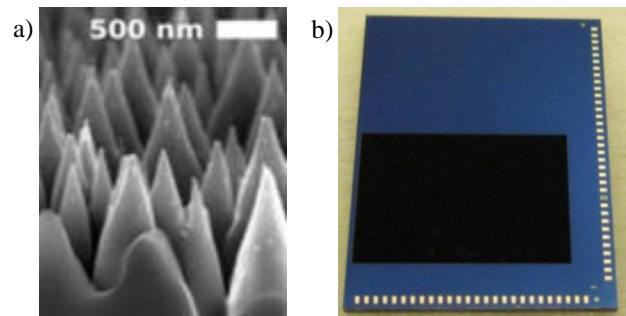


Figure 1. (a) electron micrograph of the nano-black surface, reproduced from [2], (b) nano-black layer on lower half of a CIS115 sensor

This work was funded by the European Space Agency (ESA) under contract No. 4000135291/21/NL/GLC/ov (Nano-Black Coating on Silicon CMOS Image Sensors for Extreme Sensitivity)

process was performed on only one half of the pixel array surface, the other half having the control CIS115 BSI passivation consisting of a shallow boron implant, laser anneal and anodization, but coated with the 20 nm  $\text{Al}_2\text{O}_3$  layer and having no AR coating.

During all measurements, the sensors were mounted in a vacuum chamber, and the temperature was controlled to 20 °C with a stability within  $\pm 0.05$  °C, using a water-cooled thermoelectric cooler (TEC).

## II. EXPERIMENTAL RESULTS

### A. QE measurements

Quantum efficiency (QE) is the percentage ratio of the number of photogenerated electrons  $N_e$  measured for a given number of incident photons  $N_p$  of specified wavelength  $\lambda$ :

$$QE(\lambda) = \frac{N_e(\lambda)}{N_p(\lambda)} \times 100\%. \quad (1)$$

QE measurements were taken in the wavelength range 300 nm to 1100 nm, in 20 nm steps, following a procedure established for a previous work [4]. Ten images were averaged for each measurement to reduce noise. Dark images were subtracted from lit images at each wavelength. Because of the wavelength-dependency of the intensity of the light source, the throughput of the optical components, and the device QE, integration times were optimised for each wavelength to keep the signal below saturation (ideally at  $\frac{1}{2}$  full well capacity) and for low signals the integration time was limited to 25 s, to prevent dark current becoming significant.

To perform the QE measurement, the optical system was assembled as shown in Fig. 2. An aperture mask was positioned in front of the sensor, its circular opening was offset from the pixel-array centre, and depending on the orientation of the clamp, the aperture could be either in the upper or lower half of the pixel array. The diameter of the beam reaching the sensor was chosen so that only negligible numbers of photons fell outside the edge of the pixel array.

A measurement with photodiode #2 behind the aperture in the focal plane of the DUT was used for reference measurements. The photodiode active area (with 9.5 mm diameter) was overlaid on the sensor image to check the beam position and was used as the region of interest (ROI) for QE calculations. Because the vast majority of the photons are concentrated within the aperture region, which is smaller than the photodiode area, the DUT and photodiode #2 capture the same number of photons. For calibration, readings from reference and monitor photodiodes were recorded simultaneously and used to calculate the throughput ratio (at each wavelength) of the focal plane versus the monitoring

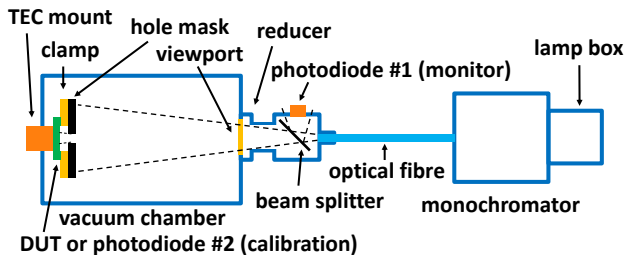


Figure 2. Experimental setup for QE measurements, for PRNU the beam splitter was replaced by a 50% ND filter

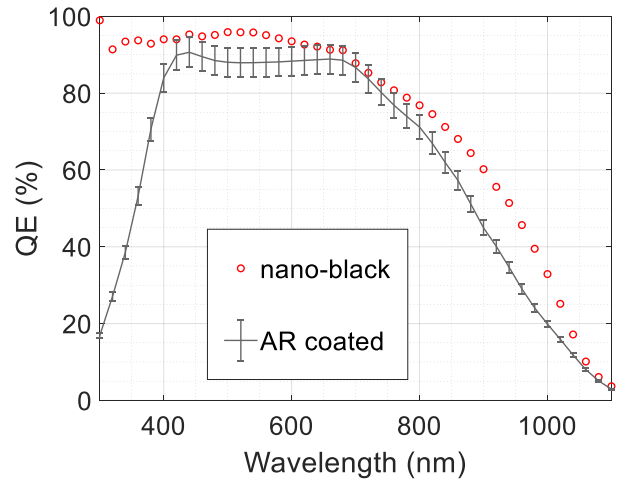


Figure 3. QE results, comparing a nano-black sensor (red circles) to the control AR coated sensor (gray curve with error bars).

location (at the beam splitter) i.e. photodiode #2 : photodiode #1. This was then used to infer the power density of photons at the focal plane from photodiode #1 readings taken whilst the DUT was in position.

A nano-black sensor is compared to the AR coated control in Fig. 3. The experimental error in the QE results is about 4%, as indicated by error bars for the control sensor (error bars are not shown for the nano-black sensor to aid clarity). The nano-black QE results are higher across most of the wavelength range, but the increase in QE is greatest at the UV end of the spectrum, because for the AR coated sensor the QE drops sharply for wavelengths below 400 nm. QEs greater than 100% are a result of higher quantum yield, i.e. more than one electron generated per photon which occurs for wavelengths below  $\approx 330$  nm.

### B. X-ray calibration

An X-ray calibration of system-gain was performed for each sensor, using an Fe-55 source, taking an average of 1000 frames collected using an integration time of 2 s, with dark frames subtracted. The system-gain was used to convert the digital numbers (DN), output by the electronics, to the number of electrons that were collected in each pixel. System-gain was close to 1.8 DN/electron for all the sensors tested.

### C. Photoresponse non-uniformity (PRNU)

For the PRNU measurements, the optical setup was modified from that shown in Fig. 2 to obtain an improved flat-field illumination. The beam splitter of the QE setup was removed because it had a fine speckled pattern of reflective material (for wide bandwidth of reflectivity) which caused non-uniform illumination. A neutral density (ND) filter was used instead, with a 50% transmission to match the previous beam splitter. The PRNU is a measure of how the pixel signal varies across the pixel array for a flat-field illumination. In practice it is difficult to achieve perfectly flat-field illumination, so a local moving mean was taken of the surrounding pixels in a  $25 \times 25$  pixel square. The measurements mostly used monochromatic illumination at a wavelength of 500 nm, except for the wavelength sweep results of Fig. 5. Ten images were averaged for each measurement to reduce noise and dark images were subtracted from lit images.

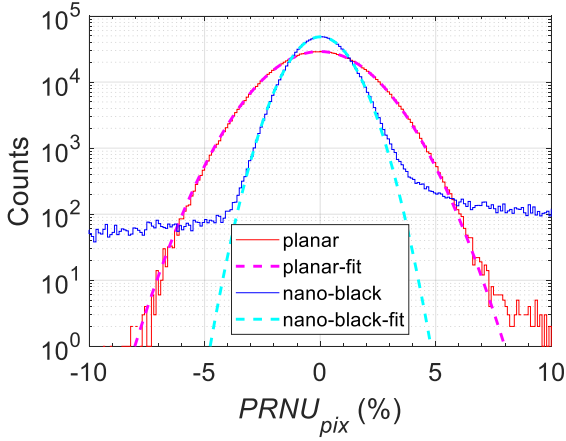


Figure 4. Histogram of  $PRNU_{pix}$  for planar and nano-black regions of sensor with gaussian fits

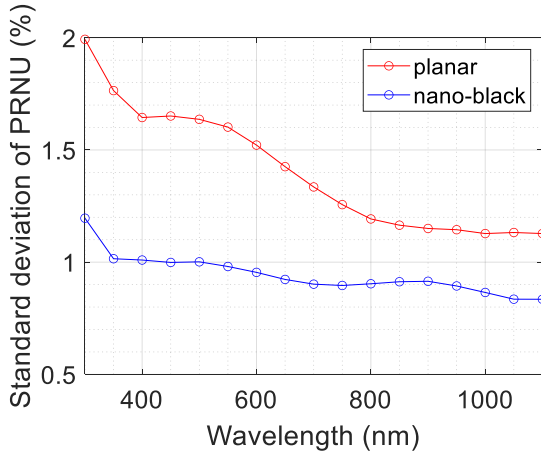


Figure 5.  $PRNU$  versus wavelength for sensor, showing comparison of the planar and nano-black regions.

The  $PRNU_{pix}$  contribution of each pixel was calculated according to [5] ignoring the first 4 rows and cols of the image area:

$$PRNU_{pix} = \frac{V_{si} - V_a}{V_a} \times 100\% \quad (2)$$

where  $V_{si}$  = individual pixel signal and  $V_a$  = local mean signal. The sensor  $PRNU$  was calculated from the standard deviation of a Gaussian fit to the  $PRNU_{pix}$  histogram, to reject the non-gaussian data of defective pixels. The lit images were taken in the linear range of operation, for an integration time of 0.7 s, corresponding to about 1/2 full well capacity.

Measurements were taken using a sensor divided into two regions, with a nano-black surface for one half and the planar control BSI passivation (without AR coating) for the other half of the chip. The  $PRNU_{pix}$  for the two regions is shown using histograms in Fig. 4. The standard deviation of the Gaussian fits, giving the sensor  $PRNU$  were 1.0% for the nano-black region and 1.8% for the planar region. The nano-black histogram has higher shoulders (at a count of around 100) where the distribution becomes non-Gaussian because of a scratch in the surface causing more defective pixels (this scratch can be seen in the dark current pixel map of Fig. 6).

The sensor  $PRNU$  was also measured for varying wavelength as shown in Fig. 5. The  $PRNU$  is lower at all wavelengths for the nano-black region of the chip, compared

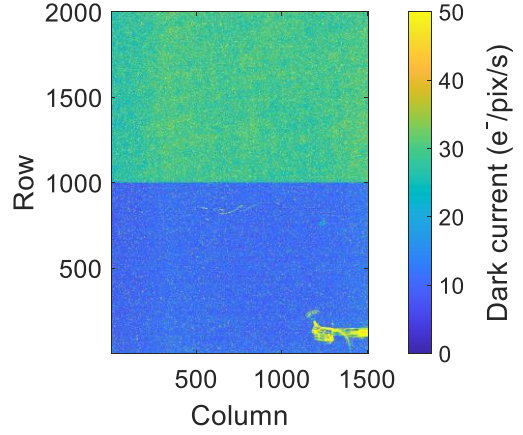


Figure 6. Dark current pixel map of sensor. Upper half: planar; lower half: nano-black

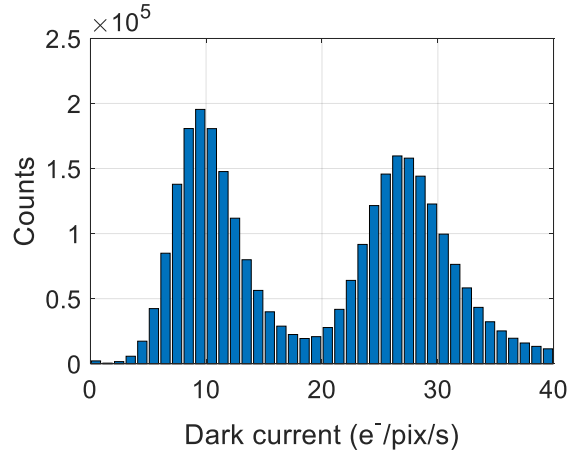


Figure 7. Dark current histogram at 20 °C of full pixel array, showing the nano-black region (left peak) and the planar region (right peak).

to the planar region.  $PRNU$  is highest for both regions at the shortest wavelengths.

#### D. Dark Current

Ten images were taken for each of a set of integration times (between 0.1 s and 1 s), the first image was rejected to eliminate effects of lag and the median was taken of the other nine, the order of the varying integration time images was also randomised to reduce systematic errors. This process was repeated three times and further averaged to suppress noise. Using the X-ray calibration, the dark current for each pixel was converted to units of  $e^-/\text{pix}/s$ .

The dark current was measured at 20 °C using a sensor which had half of its surface with the nano-black process, the other half had a planar surface with the control BSI passivation consisting of a shallow boron implant and anneal, but no AR coating. Fig. 6 shows a pixel map of the dark current for the sensor. In Fig. 7, the histogram of pixel signals from the sensor has 2 peaks, at 9 and 27  $e^-/\text{pix}/s$  for the nano-black and planar regions, respectively. These results show that the nano-black region clearly has lower dark current than the planar region.

### III. SUMMARY & CONCLUSIONS

When compared to the control CIS115s, with a conventional multilayer AR coating, the nano-black sensors

had higher QE for most of the wavelength range measured (300 nm to 1100 nm), but the greatest improvements were for UV (below 400 nm) and NIR (from 700 nm to 1100 nm) wavelengths.

The high QE at short wavelengths is consistent with results for discreet nano-black photodiodes [2] and is attributed to a combination of low reflectivity, good absorption and a quantum yield greater than one, i.e. more than one electron produced per photon. The control CIS115's AR coating was not UV optimised, which contributes to its sharp cut-off in QE below 400 nm. Also, its conventional back surface passivation is thicker than the nano-black's Al<sub>2</sub>O<sub>3</sub> passivation, so the thin Al<sub>2</sub>O<sub>3</sub> layer may in-part be responsible for the improved QE in the UV.

For high QE in the NIR, a relatively thick active silicon is required. The CIS115 is only 10 µm thick, which is approximately equal to the absorption length at 800 nm wavelength, and explains the drop-off in QE beyond 700 nm. The relative improvement in QE in the NIR for the nano-black sensor is despite the approximate 1 µm thinning of the silicon by the nano-black etching process, which would normally reduce the QE. However, some of this improvement may be attributed to increased light scattering, as indicated by the reduced PRNU.

Dark current and PRNU were reduced in nano-black sensors compared to a conventional planar BSI control. Dark current was 33% of that for the planar control. PRNU was 55% of that for the planar control.

We believe that the low PRNU of the nano-black surface compared to the planar surface is indicative of increased scattering of light, which smooths-out non-uniformities between pixels. The higher QE of the nano-black surface, particularly at longer wavelengths where the QE improvement is more modest, could also be related to the reduced PRNU because scattering could result in an increased probability of

light transmission at the surface and may also be detrimental to spatial resolution.

In this work it was shown, for first time, that the nano-black process can be used in place of conventional AR coatings for CMOS image sensors, and can be performed as a final step after CMOS fabrication and back-thinning. The commercial viability of the nano-black process depends upon addressing concerns about the ability to clean a non-planar surface and difficulties in handling during packaging, but the improved QE and reduced dark current are good reasons to further pursue this technology.

#### ACKNOWLEDGMENT

The authors thank Simon Pyatt of The University of Birmingham, UK for wire-bonding of the image sensors.

#### REFERENCES

- [1] Teledyne-e2v datasheet SIRIUS – CIS115 Back Illuminated CMOS Image Sensor [A1A-785580] Version 3, Feb 2019.
- [2] M. Garin, J. Heinonen, L. Werner, T. P. Pasanen, V. Vähänissi, A. Haarahiltunen, M. A. Juntunen, and H. Savin, "Black-Silicon Ultraviolet Photodiodes Achieve External Quantum Efficiency above 130%", *Physical Review Letters* 125, 117702 (2020).
- [3] J. Heymes, M. Soman, T. Buggey, C. Crews, G. Randall, A. Gottwald, A. Harris, A. Kelt, U. Kroth, I. Moody, X. Meng, O. Ogor, and A. Holland "Calibrating Teledyne-e2v's ultraviolet image sensor quantum efficiency processes", *Proc. SPIE 11454, X-Ray, Optical, and Infrared Detectors for Astronomy IX*, 114541G 13 December 2020.
- [4] C. Crews, M. Soman, E. A. Allanwood, K. Stefanov, M. Leese, P. Turner, and A. Holland "Quantum efficiency of the CIS115 in a radiation environment." *X-Ray, Optical, and Infrared Detectors for Astronomy IX*. Vol. 11454. 114540E International Society for Optics and Photonics, December 2020.
- [5] *Electro-optical Test Methods for Charge Coupled Devices*, ESCC Basic Specification No. 25000, issue 2, January 2014.